



OPEN Field-based experimental investigation of energy and exergy performances of a novel solar thermal air collector

Muhammad Aqil Afham Rahmat^{1,2}, Adnan Ibrahim^{1✉}, Khaled M. Al-Arife³, Ubaidah Syafiq¹, Muhammad Amir Aziat Ishak⁴, Sahibzada Imad Ud Din¹, Mohamad Arif Mokhtar¹, Norasikin Ahmad Ludin¹ & Ahmad Fazlizan¹

An energy crisis is a significant concern, and solar collectors are among the most efficient energy conversion devices. Inefficient heat transfer is an issue that reduces overall performance. This research investigates the use of hollow semi-stadium fins (HSSF) arranged in a multi-level array with baffles to enhance the system's overall performance. Outdoor testing was undertaken over three days with varying flow rates of 0.01 kg/s (Day 1), 0.03 kg/s (Day 2), and 0.07 kg/s (Day 3). The study considered the temperature of the solar collector, as well as its energy and exergy performance. The study found a thermal efficiency range of 12.99–71.91% and a maximum value of 71.91% corresponding to an irradiance of 800 W/m² and a flow value of 0.07 kg/s. The inlet-to-outlet temperature differential peaked at 21.80 °C at 0.01 kg/s. The most excellent exergy efficiency was 17.06% at a flow rate of 0.01 kg/s, with a range of 0.55% to 17.06% for all irradiances and mass flow rates. Performance results were validated using numerical results and earlier research. Larger flow rates increase thermal efficiency but decrease exergy efficiency. The solar collector with HSSF and baffles highlights its energy and exergy enhancements for sustainable energy applications.

Keywords Solar air collector, Fins, Baffles, Experimental analysis, Energy analysis, Exergy analysis

Abbreviations

HSSF	Hollow semi-stadium fins
FPSAC	Flat plate solar collectors
IEA	International Energy Agency
SDG	Sustainable development goals
PCM	Phase change material

Latin symbols

T_o	Outlet temperature
T_i	Inlet temperature
T_a	The temperature of the ambient
T_b	Bending temperature
T_{pm}	Absorber plate temperature
\dot{m}	Mass flow rate of air
m	Meters
cm	Centimeters
mm	Millimeters
kg/s	Kilogram per second
C_p	Specific heat capacity
Q_u	Useful thermal energy

¹Solar Energy Research Institute, Universiti Kebangsaan Malaysia, 43600 Bangi, Selangor, Malaysia. ²Department of Biological and Agricultural Engineering, Faculty of Engineering, Universiti Putra Malaysia, 43400 Serdang, Selangor, Malaysia. ³Department of Mechanical and Industrial Engineering, Abu Dhabi University, PO Box 59911, Abu Dhabi, UAE. ⁴School of Engineering, Faculty of Innovation and Technology, Taylor's University, 47500 Subang Jaya, Malaysia. ✉email: iadnan@ukm.edu.my

W	Watts
kW	Kilowatts
A_c	Collector area
A_s	Cross-sectional area of the collector
I	Irradiance
h_w	Convective heat transmission coefficient
ρ	Density
k	Thermal conductivity (insulation)
L_d	Duct collector length
L	Thickness (insulation)
D_h	The hydraulic diameter of a solar collector
k_{fluid}	Thermal conductivity of fluid
$Ex_{destruction}$	Exergy destruction
$E_{in,f}$	Rate of exergy input
$E_{in,Q}$	Radiation exergy rate
S_{gen}	Entropy generation rate
$E_{out,f}$	Rate of exergy output
Re	Reynolds Number
Nu	Nusselt Number
w	Duct collector width
d	Duct collector height
f	Friction factor
V	Air velocity
W_B	Baffle width
L_B	Baffle length
Greek symbols	
η_{th}	Thermal efficiency
η_{ex}	Exergy efficiency
β	Tilt angle of solar collector

The global energy sector is currently facing a critical challenge due to the increasing energy demands in industries such as transportation, electricity, and heating, as well as the rapid growth of the global population^{1–3}. According to projections, worldwide energy use is expected to increase by 33% by 2040^{4,5}. Fossil fuels, including coal, petroleum, and natural gas, currently dominate the energy production sector. At the same time, these resources are finite and significantly influence environmental degradation, particularly through carbon dioxide emissions that contribute to adverse climate change^{6,7}. In contrast, solar energy offers a sustainable and renewable alternative that can meet energy needs indefinitely, while simultaneously reducing pollution levels and minimizing environmental damage^{8–10}. The burning of fossil fuels currently accounts for nearly 80% of global energy, according to the International Energy Agency (IEA). This dependence is envisioned to persist, with an anticipated yearly growth rate of 0.9% by 2030¹¹. In the meantime, renewable energy technologies are undergoing rapid development, with a foreseen yearly expansion rate of 3.0% up to 2030^{12–14}.

A solar thermal collector device serves as a substitute energy solution and is recognized as a green technology, contributing to reduced fossil fuel utilization and mitigating environmental pollution¹⁵. The flat plate solar collector (FPSC) is a notable technology used in solar energy systems to convert solar energy into thermal energy^{16,17}. The collector's setups incorporate numerous airflow designs. According to the application, solar collectors can be categorized into single-pass, double-pass, and triple-pass systems^{18,19}. Fudholi et al.²⁰ found that the solar air flat plate collector's energy and useful work potential performances fluctuated between 28 and 62% as well as 30% and 57%, respectively, making it suitable for drying applications. Azha et al.²¹ also found that collectors may heat water.

FPSCs are a favored choice for solar energy applications due to their cost-effectiveness, simplicity, and flexibility. Nevertheless, the core issue with FPSC is the inefficient heat exchange rate between the absorbent plate component and the circulation, which substantially decreases performance^{9,22,23}. The issue can jeopardize the utilization of FPSC in various sectors. This is because it impacts the FPSC's technical performance and feasibility for real-world applications. In light of this, the FPSC's overall performance is enhanced by combining fin technology and baffle technology. The advancement of solar air collectors represents a deliberate initiative aimed at fulfilling Sustainable Development Goal (SDG) 7: Ensuring Affordable and Clean Energy^{15,24}. The SDG highlights the importance of embracing energy technologies that are environmentally sustainable, economically viable, and renewable²⁵. Solar thermal devices are critical in this context, facilitating the revolution to clean, affordable, and sustainable energy solutions. Next, Obaideen et al.²⁶ indicate that approximately 72% scientific publications within the domain of solar energy technologies are linked to Sustainable Development Goal 7. Moreover, incorporating solar energy systems is gaining recognition as crucial in promoting global initiatives for sustainability and achieving net-zero carbon emissions^{27,28}. Panda et al.²⁹ discovered that the deployment of solar energy in the agricultural and aquaculture sectors can contribute to the realization of numerous United Nations Sustainable Development Goals (SDGs).

Various solutions are applied to elevate the potency of solar air devices^{30,31}. A considerable amount of crucial studies have focused on the use of baffles and fins in solar collectors. Rani et al.³² demonstrated that applying fins along with baffles in solar collectors augmented thermal performance by up to 2.67 times and enhanced thermal efficiency by approximately 19.73% to 34.3%. This was achieved while concurrently reducing pressure drop and significantly improving heat transfer coefficients across diverse flow rates. A thermal performance boost of up to

44% over a smooth channel was observed by Jamal et al.³³, who demonstrated that the implementation of equally shaped fins with minimum spacing, especially at half the fin's length, leads to a considerable improvement in heat transfer and flow dynamics inside the solar air heater. Boussouar et al.³⁴ found that perforated baffles featuring two openings, each with a diameter of 15 mm and a thickness of 1–2 mm, exhibited the highest Nusselt number (up to 79.56) and a pressure drop of approximately 459–496 Pa at a Reynolds number of 8500, thereby optimizing heat transfer efficiency. Razali et al.³⁵ found that multidirectional tapered fins outperform rectangular fins by over 10% in solar collector performance. Past research has demonstrated that the inclusion of baffles and fins significantly improves the efficiency of solar air collectors.

Experimental testing of FPSAC is necessary for evaluating its real-time performance. As a result, solar thermal technologies have been the subject of numerous studies over the years, evaluating their performance and feasibility by examining their exergy and energy aspects. The collector developed by M. Arun³⁶ achieved an exergy efficiency of 21.18% and an energy efficiency of 81.57% at a nanofluid concentration of 0.1 wt%, thereby enhancing its performance. Brahma et al.³⁷ indicated that the solar air collector in the solar dryer incorporating phase change material (PCM) achieves an efficiency of energy ranging from 50.77% to 78.41%, along with an exergy efficiency of approximately 2.66% to 2.94%, thereby markedly enhancing drying performance compared to conventional open space drying techniques. Madadi et al.³⁸ proved that the use of nanofluids significantly improves the energy efficiency of solar thermal systems by 25%. Besides that, Din et al.¹⁶ assessed a double-pass design combining vertically oriented PCM cylinders arranged in a staggered sandwich configuration, achieving an experimental thermal efficiency of up to 90.97%, particularly at lower mass flow rates of 0.01–0.03 kg/s, by enhancing heat transfer and energy storage through increased contact area and turbulence enhancement.

Although many investigations have examined the effectiveness of various solar collector configurations, there has been a lack of focus on the synergistic effects of baffles and hollow fin designs in multi-level set distance arrangements within solar thermal air collectors with a double-pass configuration, particularly concerning energy and exergy aspects through outdoor experimental testing. Filling this gap is essential for enhancing the overall operational performance of these technologies. Consequently, additional investigation in this domain is necessary. This paper aims to analyze the energy and exergy effects of the flat plate solar air collector (FPSAC) utilizing a multi-level array configuration of hollow semi-stadium fins (HSSF) with baffles. Comprehensive performance analyses (energy and exergy) are conducted to evaluate the effectiveness of this collector. This study presents a novel approach by incorporating a semi-stadium fin shape with a hollow design within a multi-level array in the solar absorber of the collector. Based on the literature, this investigation is an extensive and experimental study. The primary contributions of the study are outlined as follows:

- A layered design featuring HSSF and baffles, as implemented in the FPSAC, improves its overall performance. To optimize system performance, fins are configured with a multi-level array with spacing differences of 1:2 and tested in real-time conditions.
- For energy analysis, the heat exchange rate of the device significantly enhances the thermal energy conversion of the FPSAC through its distinctive use of HSSF integrated with baffles.
- The system exhibits a significant enhancement in exergy performance by reducing irreversibility in heat transfer processes. This improvement is attributed to the presence of a fin and baffle configuration, which results in more sustainable thermal energy utilization.
- A comprehensive assessment framework that includes energy and exergy performance is presented, with results validation demonstrating excellent agreement with previous research findings.

Methodology

The field-based assessment commences with the setting up of the solar collector through the assembly of the HSSF and baffles, followed by outdoor testing. Data are subsequently analyzed about energy performance, exergy performance, and comprehensive collector temperature behavior. Finally, both the numerical and experimental results are compared to validate the findings before concluding the study. The flowchart illustrating the investigation is presented in Fig. 1.

Novel fins and system description

Fins significantly improve the thermal energy utilization of collectors^{18,39}. The solar collector used in this research uses novel stainless steel fins organized in a multi-level gap array with a hollow semi-stadium form. Figure 2 depicts the novel fins, indicating that they possess a distinctive structure resembling a semi-stadium. The fin has been enhanced based on prior research indicating the importance of optimizing design characteristics to improve flow and thermal effectiveness^{40,41}. The dimensions of these fins are as follows: height measures 4 cm, fin thickness is 0.3 cm, width is 3 cm, and hollow thickness is 0.5 cm.

Figure 3a shows a modified FPSAC with a revolutionary thermal improvement approach. The absorber plate has multi-level gap hollow semi-stadium stainless steel fins (HSSF) with baffles. Fins are strategically positioned to enhance heat interaction and ventilation dispersion. Baffles near the inlet section mix and guide incoming air to improve its contact with hot surfaces. A double-pass counterflow optimizes heat absorption from the absorber plate when airflow enters from the bottom, travels through the finned zone, and departs via the outlet. Air passes via the higher and lower ducts in the collectors. HSSF and baffles are attached to the top duct, located between the glazing and the absorber plate. The reverse air movement direction is positioned at the lower area of the duct, between the HSSF absorber plate and the collector bottom frame. A U-shaped bending area that connects the upper and lower ducts.

The solar absorber has a length and width of 2.3 m and 0.54 m, with a material thickness of 3.5 mm. It is made of black-painted aluminium. The upper and lower air passages of the system are deep, measuring 0.063 m and 0.07 m, respectively. Softwood blocks with thicknesses of 4.0 cm and 2.5 cm have been affixed to the sides

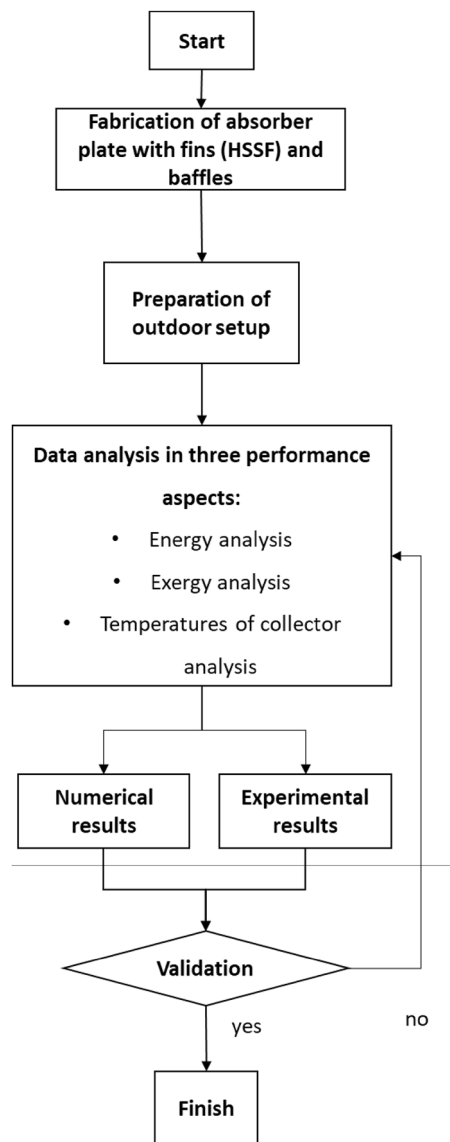


Fig. 1. Flowchart of the field-based study.



Fig. 2. Hollow semi-stadium fins (HSSF) structure.

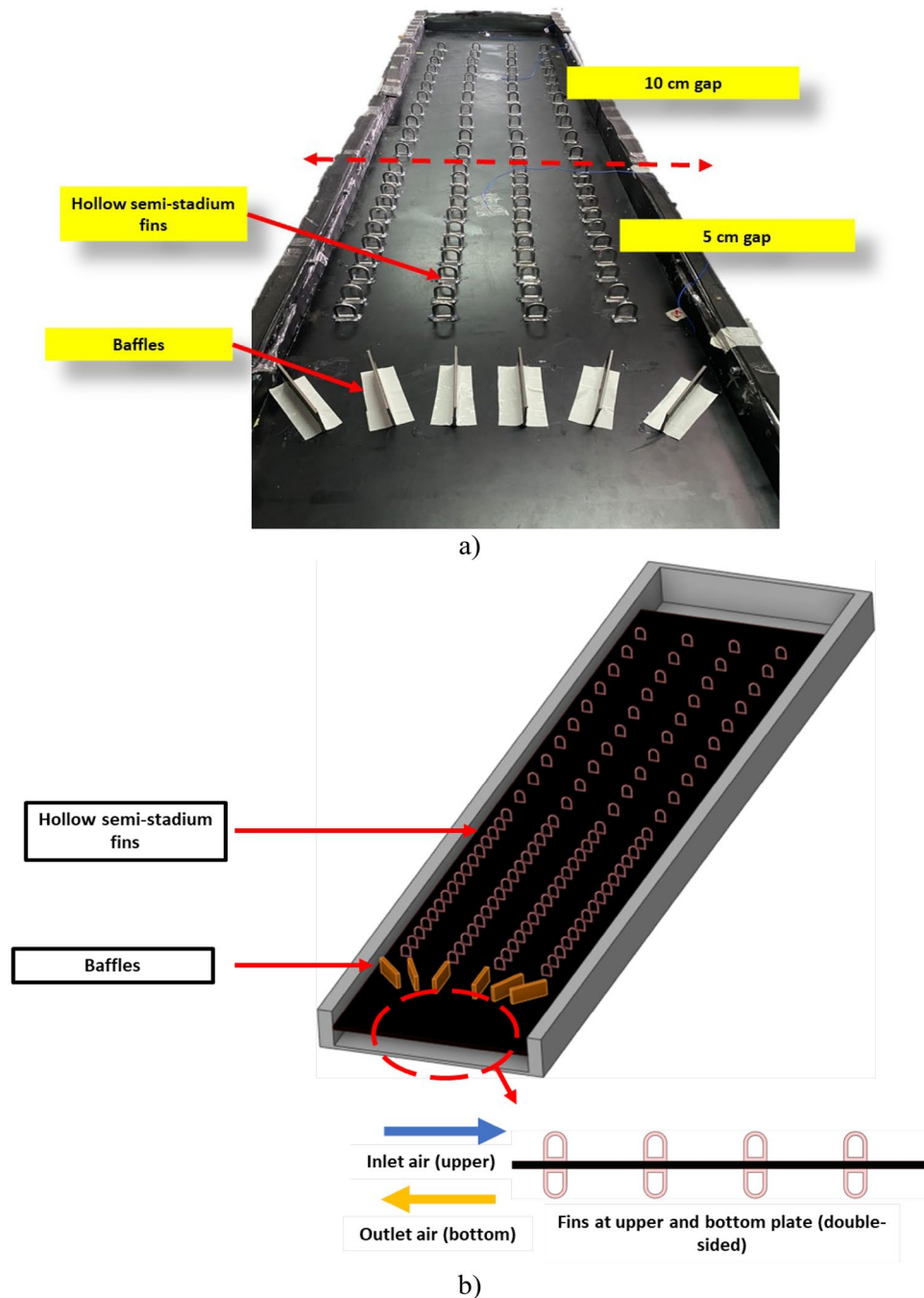


Fig. 3. (a) Overview of FPSAC added with HSSF (multi-level array), and baffles at the absorber plate, and (b) 3D model of FPSAC.

and bottom of the conduits to provide insulation. A separation of 0.063 m is established between the absorbent plate and the glass surface by placing a 4.3 mm thick glass cover above the upper duct. The galvanized iron (GI) conduit is used to affix a 0.75 kW air vacuum at the outlet section. The solar simulator is situated 1.5 m above the solar collector. Table 1 provides a summary of the collector's specifications, while Fig. 3b illustrates the FPSAC system's operational concept and design model, which includes innovative fins and baffles.

Experimental procedure

The experimental setup considered for the field-based investigation is an FPSAC with a multi-level array of HSSF and baffles. Following the research conducted by Ng et al.⁴², the solar collector is positioned with an inclination angle of 15° to facilitate rain discharge in a south-facing direction, guaranteeing optimal solar exposure throughout the day. The FPSAC functions as the energy conversion unit that captures solar radiation to heat air as it travels through two distinct passages, thereby improving heat transfer efficiency. Environmental factors,

Solar collector parts	Details	Values
Collector	Width × length × height, cm	54 × 230 × 17
Glazing	Emittance	0.85
Flat plate	Emittance	0.20
Air suction	Load, kW	0.75
Fins	Height dimension, cm	4
	Width dimension, cm	3
	Length dimension, cm	0.3
	Hollow thickness dimension, cm	0.5
Baffles	Height dimension, cm	5
	Width dimension, cm	10
Insulation	Thermal conductivity, W/Mk	0.0262
	Material thickness, cm	4

Table 1. Solar collector design parameters.

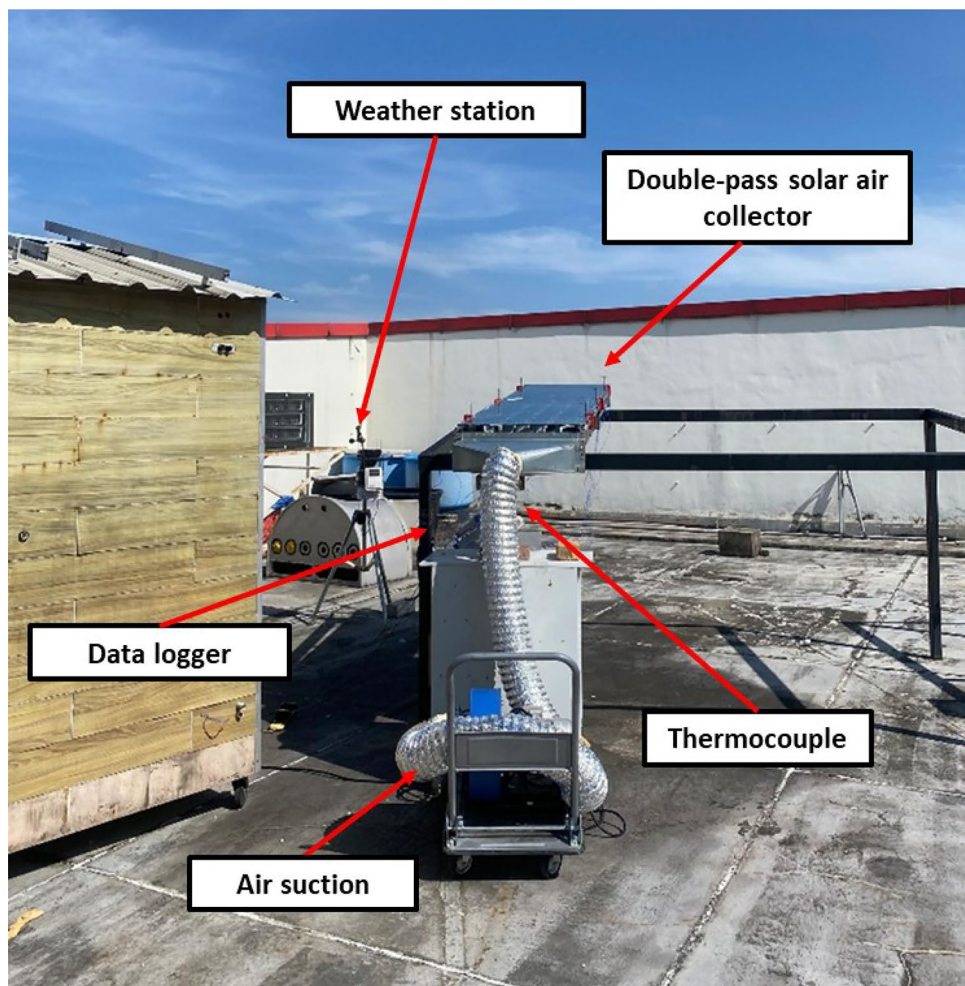


Fig. 4. Outdoor experimental setup.

including solar irradiance, wind speed, and ambient temperature and humidity, are monitored by a weather station. Thermocouples were installed at numerous locations along the air collector and ducting. Continuous data acquisition over time was achieved by employing a data recorder to record data from thermocouples. The airflow rate was controlled by the air suction, which allowed for the analysis of various flow conditions. Figure 4 illustrates the outdoor experimental setup.

Three mass flow rates of air are utilized to conduct outdoor testing. The experiments were conducted for three days at varying flow rates (0.01 kg/s, 0.03 kg/s, and 0.07 kg/s). After executing the indoor experimental testing,

Outdoor experiment	
Parameters	Values
Mass flow rate, kg/s	0.01 (Day 1), 0.03 (Day 2), 0.07 (Day 3)
Time	09:00 AM to 04:00 PM
Days of experiment	Three days (Day 1, Day 2, and Day 3)
Specific capacity of air C_p , J/kgK	1006
Density of air, kg/m ³	1.225
Location coordinate	2°55'38.4"N 101°46'05.3"E
Location detail	Solar Energy Research Institute, Universiti Kebangsaan Malaysia (UKM), Bangi, Malaysia
Inclination angle	15°

Table 2. Outdoor experimental parameters and conditions.

Instrument	Variables	Instrument model	Measuring range	Units	Uncertainties, %
Thermocouples	Temperature	K-type	-200—1260 °C	°C	± 0.1
Data logger	Temperature readings	AT4808 data taker	-200—1300 °C	°C	± 0.1
Anemometer	Velocity	AM4206	0.40—25.0 m/s	m/s	± 1.2
Air Suction	Velocity	GTG GCIL 200	-	m/s	± 1.1
Weather station	Irradiances	Vantage Pro2 Plus	0 ~ 1800 W/m ²	W/m ²	± 5%
Weather station	Ambient temperature	Vantage Pro2 Plus	-79 ~ 93 °C	°C	± 0.3 °C
Weather station	Humidity	Vantage Pro2 Plus	0.1 ~ 100%	%	± 2%

Table 3. Measuring instrument uncertainties.

these three airflow rates were selected as the most significant flow rates affecting the collector's performance. The testing was conducted at the Solar Energy Research Institute (SERI) in Universiti Kebangsaan Malaysia (UKM) from 9:00 AM to 4:00 PM. The weather station monitored the ambient temperatures, solar irradiance, and humidity. Various air properties were employed, including a density of 1.225 kg/m³ and a specific heat capacity of 1006 J/kg·K. The collector was installed at the test location, with coordinates of 2°55'38.4"N, 101°46'05.3"E. The key environmental and operational variables that were observed during the outdoor testing of the solar air collector are summarised in Table 2. The evaluations are categorized into many aspects, such as energy performance, including usable energy and thermal efficiency, along with exergy performance, which includes exergy efficiency and exergy destruction. The temperatures of the collectors were evaluated, including the input, outlet, plate, and bending temperatures of the collectors.

Uncertainty analysis

Uncertainty analysis is a structured technique for assessing and estimating errors. To fulfil this requirement, thorough sensor calibration procedures were conducted beforehand to improve measurement precision, reliability, and the overall validity of the data. It is essential to evaluate the reliability of data by ensuring that measurements are accurate and precise. Table 3 displays the findings of determining the level of uncertainty for each component of the equipment. The analysis results demonstrated that the measurement precision and reliability were enhanced, with uncertainties less than 2%. The standard deviation is represented using Eq. 1⁴³. The mean of the measurements, the number of measurements, and the results of the measurements are represented as \bar{x} , n , x_i , and \bar{x} . The corresponding uncertainty, u , is denoted by Eq. 2.

$$s = \sqrt{\frac{\sum_i^n (x_i - \bar{x})^2}{n - 1}} \quad (1)$$

$$u = \sqrt{\frac{s}{\sqrt{n}}} \quad (2)$$

Numerical procedure

Numerical testing is employed to verify the experimental outcomes of the outdoor testing of FPSAC with HSSF and baffles. The computational fluid dynamics tool used is Ansys Fluent 23.2 software, which facilitates the investigation of heat transport and airflow phenomena inside the system^{44,45}. Numerical assumptions were established whereby the air is defined as an incompressible, Newtonian, stable, and three-dimensional medium. Furthermore, there are no thermal losses at the boundaries of the collector nor any air leakage along the solar collector. The k-ε Realizable model is utilized to analyze the correlations between heat transfer in heat conduction and fluid flow within solids in conjugate heat transfer involving turbulent flow.

The mesh independence analysis is performed utilizing six distinct grid configurations that vary from extra coarse to extra fine, as illustrated in Table 4. The geometry density of the simulations was determined through

Meshing setting (number of elements)	Values of average element quality	Variation in average element quality
Extra coarse (332,927)	0.59	9.56%
Coarser (783,331)	0.69	4.36%
Coarse (1,714,048)	0.73	2.56%
Normal (3,091,833)	0.76	1.10%
Fine (1,994,586)	0.77	0.76%
Finer (3,340,851)	0.78	-0.02%
Extra fine (3,504,321)	0.78	

Table 4. Summary of mesh independence study.

a grid independence analysis conducted using Ansys. The criterion employed was average element quality, a quantitative metric that assesses the overall quality of all elements within the mesh, including skewness, aspect ratio, orthogonal quality, and the Jacobian ratio. Minor improvements in average element quality indicate that finer meshes do not increase computational load. Further refining only lowers element quality by -0.02% , confirming mesh independence.

To validate the findings, the outdoor experimental measurements were compared with the computational fluid dynamics (CFD) simulation results, specifically regarding energy efficiency across a range of irradiance levels (400–800 W/m²) and flow rates (0.01–0.07 kg/s). Subsequently, the outdoor findings are also validated through comparison with previous studies by P. Sudhakar and M. Cheralathan⁴⁶, as well as Kim et al.⁴⁷, by analyzing the trends and thermal performance.

Energy formulations

Thermal energy is directly converted from solar radiation using a solar thermal energy conversion device. Adding the fins and baffles to the collector could increase its energy efficiency⁴⁸. This study examines the efficiency and acquisition of thermal energy by the solar thermal device. The solar collector's effective heat gain is determined by the combined mass flow rate of the working fluid, the recorded temperatures of the inlet (T_i) and outlet (T_o), and the solar irradiance. Equations 3–4^{43,49} encapsulate this relationship, with C_p denoting the specific heat capacity (air). In the interim, Eqs. 5–6^{50,51} are implemented to assess the thermal efficacy of the collector.

$$Q_u = \dot{m}C_p(T_o - T_i) \quad (3)$$

$$\dot{m} = \rho V A_s \quad (4)$$

$$E_{sun} = I A_c \quad (5)$$

$$\eta_{th} = Q_u / E_{sun} \quad (6)$$

A_c stands for the collector plate's surface area, and I stands for solar irradiation. The surface area of the collector is determined using Eq. 7¹⁹.

$$A_c = Width \times Length \quad (7)$$

Exergy formulations

Exergy analysis refers to techniques for determining the usable work potential of energy inside a system⁵². It measures energy in terms of both quantity and quality⁵³. The performance of solar thermal collectors in producing maximum useful work must be evaluated, taking into account both the quality and degradation of energy during conversion^{54,55}. The governing equations, parameters, and a detailed explanation of the FPSAC's exergy effectiveness study are provided in this section. The input exergy rate includes both the exergy from solar radiation and the exergy carried by the flowing fluid. The fluid flow rate determines the inlet exergy, which is represented by Eq. 8⁵⁶.

$$E_{in,f} = \dot{m}c_p \left(T_i - T_a - T_a \ln \left(\frac{T_i}{T_a} \right) \right) \quad (8)$$

The exergy rate of solar radiation on the collection surface is determined by Eq. 9. Where I denote solar irradiation, and A_c denotes aperture area. T_s , the apparent solar temperature known as an exergy source, is assumed to be 4350 K^{43,57}. Equation 10⁴³ defines exergy destruction, also known as $Ex_{destruction}$. The rate of output exergy transported by fluid flow is represented by Eq. 11. Next, Eq. 12 is used to describe the entropy generation rate, denoted by the symbol S_{gen} . In Eq. 13, the entire amount of absorbed solar energy is symbolized by the symbol Q_s , a useful heat gain of the solar collector system. The symbol indicates the total useful heat gained across the absorber area, taking into account optical reflection and transmission effects on the surface⁵⁴.

$$E_{in,Q} = I A_c \left(1 - \frac{T_a}{T_s} \right) \quad (9)$$

$$Ex_{destruction} = T_a S_{gen} \quad (10)$$

$$E_{out,f} = mc_p \left(T_o - T_a - T_a \ln \left(\frac{T_o}{T_a} \right) \right) \quad (11)$$

$$S_{gen} = \left[\left(\frac{1}{T_a} - \frac{1}{T_s} \right) \cdot Qs \right] + \left[\ln \left(\frac{T_{out}}{T_i} \right) - \left(\frac{T_{out}}{T_a} \right) + \left(\frac{T_i}{T_a} \right) \right] \dot{m} C_p \quad (12)$$

$$Qs = \left[\frac{I\alpha_{PV}P + I\alpha_l(1-P) + I\tau_l(1-P)n_{R\alpha_{PV}}P + I\tau_l(1-P)n_{R\alpha_{PV}}(1-P)}{I\tau_l(1-P)n_{R\alpha_{PV}}(1-P) + I\tau_l(1-P)(1-n_R)} \right] \cdot Ac \quad (13)$$

According to Eq. 14, the equations below represent the usable exergy rate. Due to that, the efficiency of exergy of FPSAC is determined by dividing the useful exergy rate by the incoming radiation exergy, as outlined in Eq. 15.

$$E_u = E_{out,f} - E_{in,f} \quad (14)$$

$$\eta_{ex} = \frac{E_{out,f} - E_{in,f}}{I A_c \left(1 - \frac{T_a}{T_s} \right)} \quad (15)$$

where $E_{out,f}$ denotes the useful exergy output of the air and $E_{in,f}$ denotes the exergy input of the air. Denoted as η_{ex} , the exergy efficiency of the FPSAC quantifies the efficiency with which the available energy (exergy) is converted into usable output.

Results and discussions

Solar irradiances and ambient temperature

Over three days, the ambient temperature and solar irradiance were monitored at various air mass flow rates (0.01 to 0.07 kg/s). Figure 5a illustrates the solar irradiance and ambient temperature ranging between 9:00 AM and 4:00 PM on Day 1, with a flow rate value of 0.01 kg/s. Irradiation increased from 234 W/m² to a maximum of 928 W/m² at 1:00 PM, followed by an abrupt decline at 2:30 PM, likely due to cloud shading, and a swift recovery. The ambient temperature increased progressively from approximately 26 °C to a maximum of 35.5 °C, exhibiting less fluctuation than irradiance due to the accumulation of environmental heat.

The ambient temperature and irradiances from Day 2 are depicted in Fig. 5b at a flow rate value of 0.03 kg/s. The solar irradiation fluctuated between 288 W/m² and 939 W/m² throughout the day due to intermittent cloud cover. The ambient temperature increased consistently from approximately 26 °C to a maximum of 33.67 °C between 2:30 PM and 3:00 PM, once again demonstrating minimal short-term fluctuation, which is indicative of the accumulated solar heating. On Day 3, the irradiance experienced a significant increase to 806 W/m² at a flow rate of 0.07 kg/s, followed by a subsequent decline to 86 W/m², attributed once again to cloud cover. This is illustrated in Fig. 5c. The ambient temperature, which fluctuated between 25 °C and 33 °C, increased progressively and remained relatively stable despite the abrupt variations in irradiance.

Thermal profile of solar collector

The thermal efficiency of solar collectors is significantly impacted by their operating conditions and design. Performance can be substantially improved through innovations such as baffles and fins. At mass flow rates of 0.01, 0.03, and 0.07 kg/s, Fig. 6 illustrates the temperature distribution of the FPSAC using a multi-level HSSF array and baffles over a period of three days. Inlet–outlet temperature differences, bending temperature, absorber plate temperature, and outlet temperature were all measured. The thermal response was evaluated by varying the airflow rates, while the collector geometry remained constant. On Day 1 in Fig. 6a, at a flow rate of 0.01 kg/s, the absorber plate recorded the highest average temperature of 53.45 °C, followed by the outflow at 50.50 °C. However, the bending temperature was lower at 33.21 °C. The largest temperature differential attained was 21.80 °C between 12:00 and 3:00 PM, indicating substantial output potential for drying or space heating.

On Day 2, as shown in Fig. 6b, at a flow rate of 0.03 kg/s, the average temperatures of the absorber plate and exit were 47.62 °C and 41.13 °C, respectively. The maximum temperature differential between the inlet and the outlet was 12.24 °C. Temperatures equilibrated at 11:30 AM. The outflow was much lower than the plate, with an average bending temperature of 30.62 °C. In comparison to 0.01 kg/s, this flow rate resulted in reduced output temperatures and diminished temperature differentials. On Day 3 in Fig. 6c, at a flow rate of 0.07 kg/s, the average temperatures of the plate, outlet, and bending were 36.10 °C, 33.73 °C, and 29.87 °C, respectively. The most significant temperature variation was just 8.69 °C, with values decreasing after 2:00 PM. Despite elevated plate temperatures, the outlet and differential values were minimal, indicating that this flow rate is more suitable for applications requiring high circulation rather than elevated discharge temperatures.

The investigation reveals that convective heat transfer is facilitated by the increment in the mass flow rate, thereby reducing excessive heating on the plate. The FPSAC's profile indicates a decrease in both the plate and outlet temperatures as the flow rate rises from 0.01 kg/s to 0.07 kg/s. The reduction of plate temperature as the flow rate increases is due to the promotion of convective cooling. This is accompanied by a decrease in the temperature differential, resulting from increased convective transmission and a shorter air residence time within the collector. Operating at a lower flow rate of 0.01 kg/s results in higher output temperatures and wider temperature differences, which is advantageous for applications that need high air temperatures, such as drying⁵⁸. Conversely, a higher flow rate value enhances heat extraction capability while reducing the rise in air temperature.

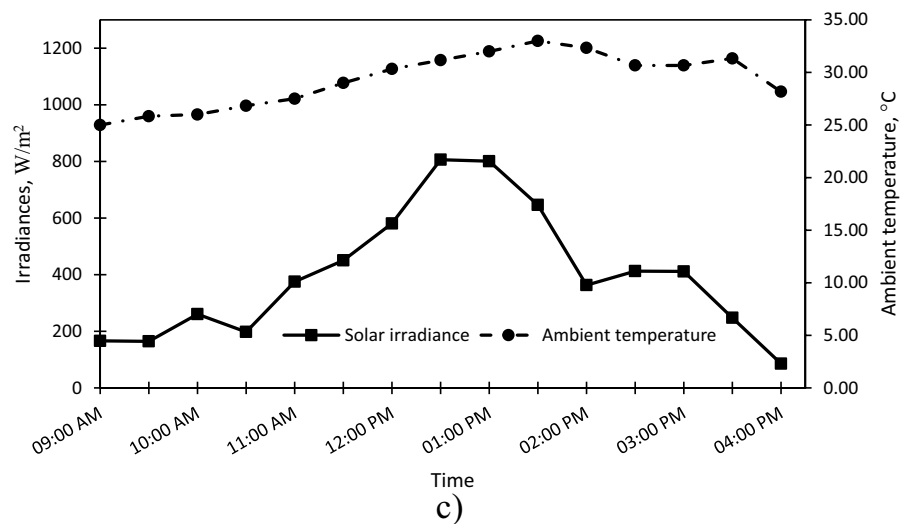
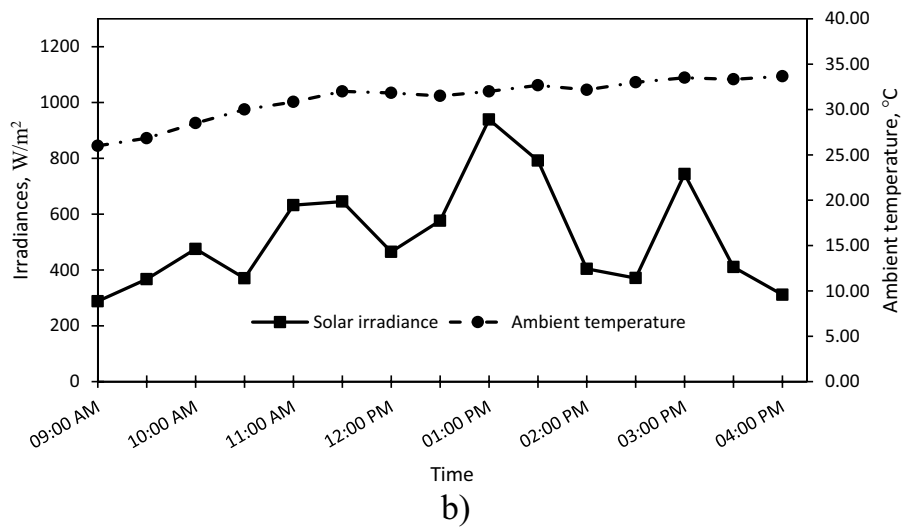
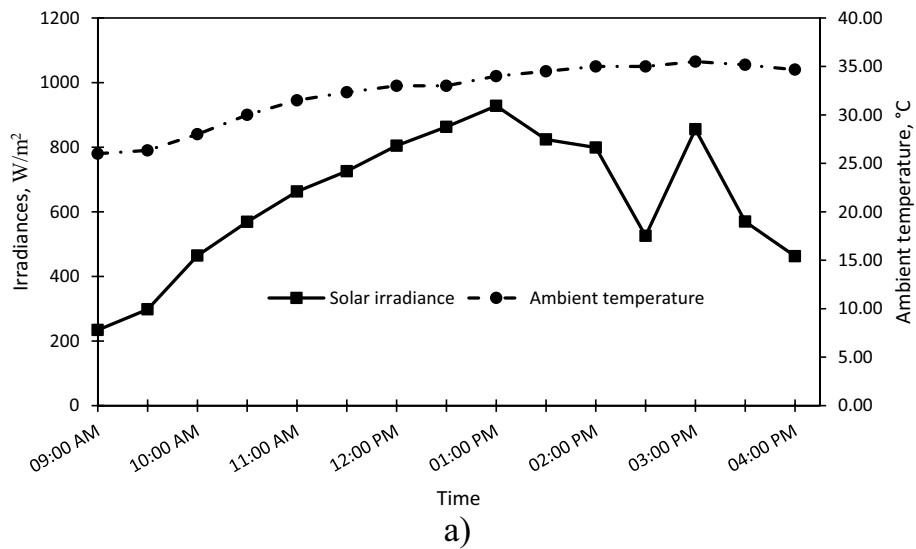


Fig. 5. Solar irradiances and ambient temperatures on three different days, along with mass flow rates. (a) Day 1 (0.01 kg/s), (b) Day 2 (0.03 kg/s), and (c) Day 3 (0.07 kg/s).

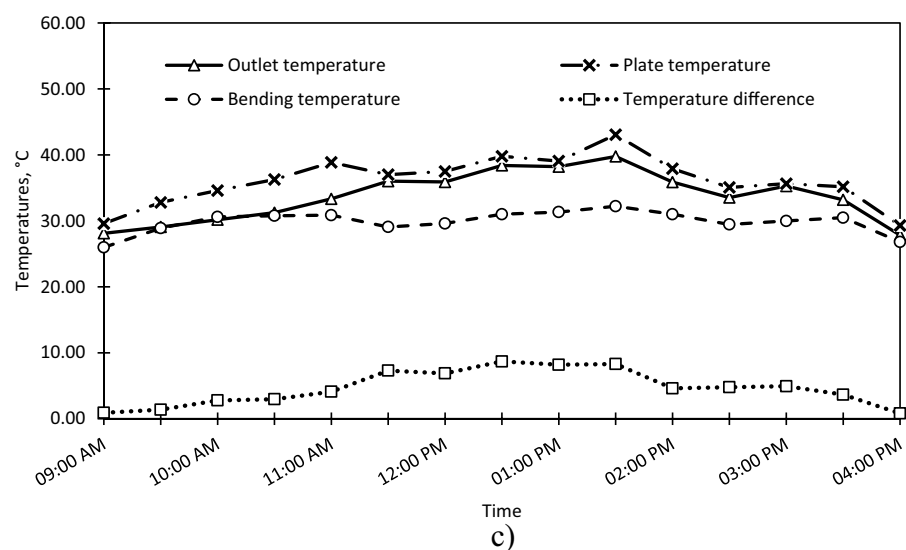
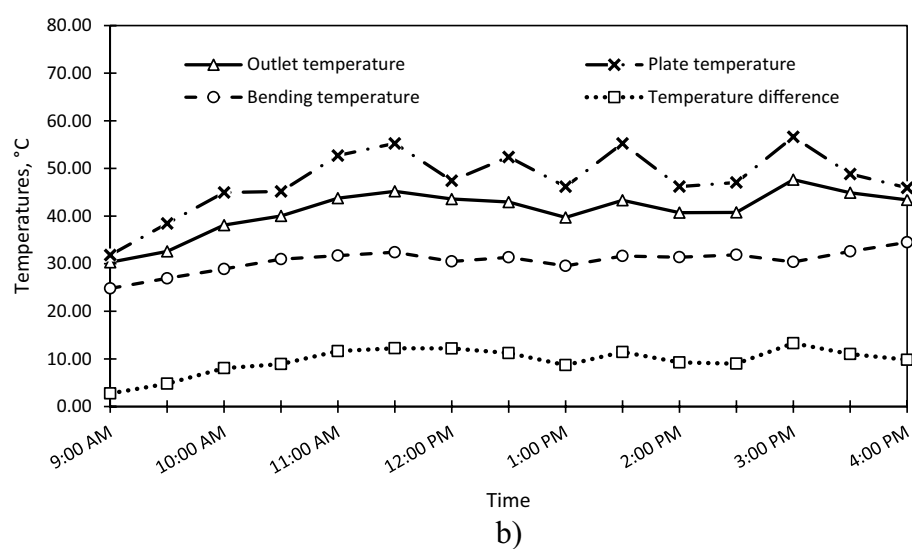
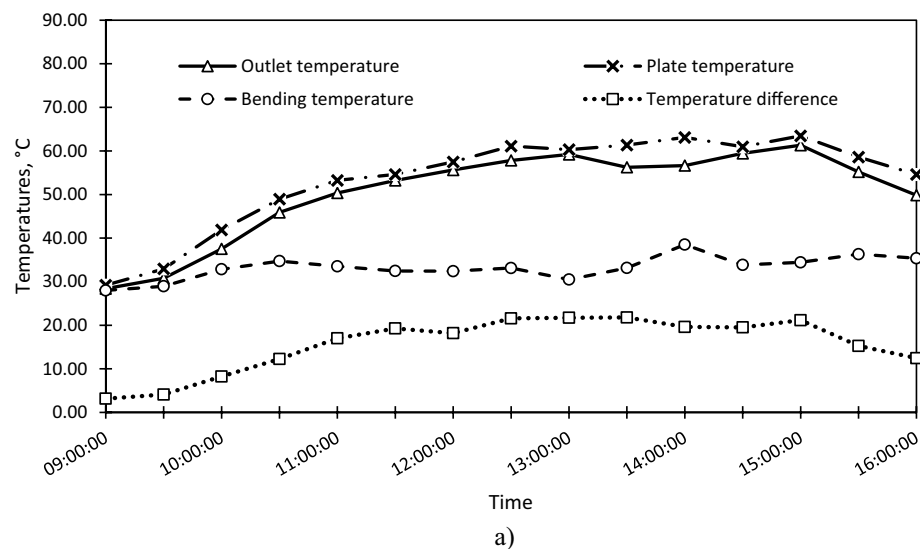


Fig. 6. Temperatures of FPSAC. (a) Day 1 (0.01 kg/s), (b) Day 2 (0.03 kg/s), and (c) Day 3 (0.07 kg/s).

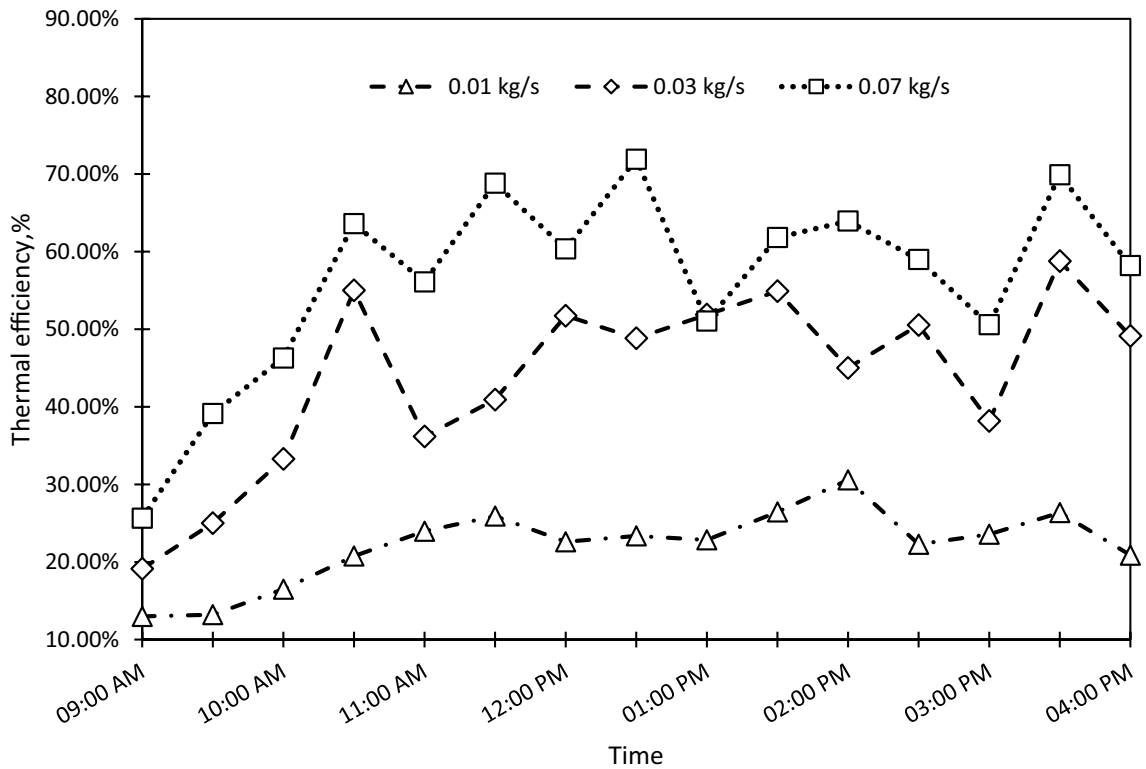


Fig. 7. Thermal efficiencies of FPSAC for three days.

Mass flow rate, kg/s	Average thermal efficiency, %	Average useful energy, W
0.01	22.15	233.07
0.03	43.90	295.91
0.07	56.42	326.87

Table 5. Overview of thermal efficiency.

Energy performance of solar collector

Energy performance in outdoor conditions is crucial for verifying the feasibility of this collector system for practical applications in real-world settings. The thermal efficiency of FPSAC using HSSF and baffles at three mass flow rates of air (0.01 kg/s, 0.03 kg/s, and 0.07 kg/s) during three individual days (Day 1, Day 2, and Day 3) is illustrated in the line graph in Fig. 7 for each day. From 9:00 AM to 10:30 AM on all days, the trend indicated an increase in thermal efficiency in the morning. After that, the thermal efficiency began to fluctuate in the afternoon due to changes in ambient temperature and solar irradiance. The most consistent efficiency is demonstrated by the 0.07 kg/s case on Day 3, with a range of 25.64% to 71.91%. The 0.03 kg/s case on Day 2, with a range of 19.145% to 58.77%, exhibits more fluctuations. The 0.01 kg/s case on Day 1, with a range of 12.99% to 30.58%, remains relatively stable but low. A highest thermal efficiency of over 71.91% is achieved at the highest flow rate of 0.07 kg/s, followed by 0.03 kg/s at 58.77%, and 0.01 kg/s at 30.58%, which stays below 40%. The reason for this is that the collector extracts more heat at higher flow rates, which in turn reduces heat losses and improves efficiency. Therefore, an increased mass flow rate of air enhances thermal energy absorption while reducing the temperature differential between the input and output of the collector. The summary of the energy performance for each flow rate is presented in Table 5 below. The table demonstrates that the average thermal efficiency increases with mass flow rate, rising from 22.15% at 0.01 kg/s to 56.42% at 0.07 kg/s. Correspondingly, the average useful energy production increases from 233.07 W at 0.01 kg/s to 326.87 W at 0.07 kg/s, indicating improved heat extraction at higher flow rates.

The highest thermal efficiency values of the FPSAC is illustrated in Fig. 8 by a bar chart, which shows the collector’s performance at different irradiance conditions (200, 400, 600, and 800 W/m²) over three days at varying flow rate values (0.01, 0.03, and 0.07 kg/s). The analysis indicates a rising trend in efficiency as flow rates increase. Based on all irradiance levels, an irradiance of 800 W/m² yields the most excellent thermal efficiency across all flow rates, with efficiency ranging from 30.58% to 71.91%. For an irradiance level of 200 W/m², the efficiency is at its lowest across all flow rates, ranging from 12.99% to 25.64%. The peak efficiency recorded during this outdoor testing is 71.91%, achieved at an irradiance of 800 W/m² and a flow rate of 0.07 kg/s, attributed to

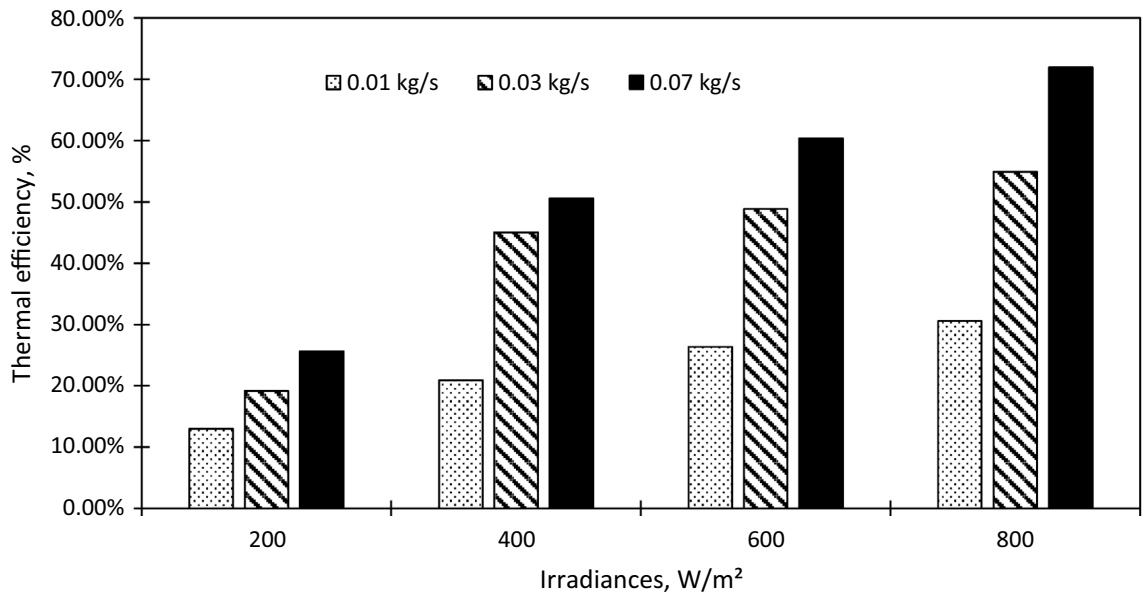


Fig. 8. Highest thermal efficiency across irradiance levels.

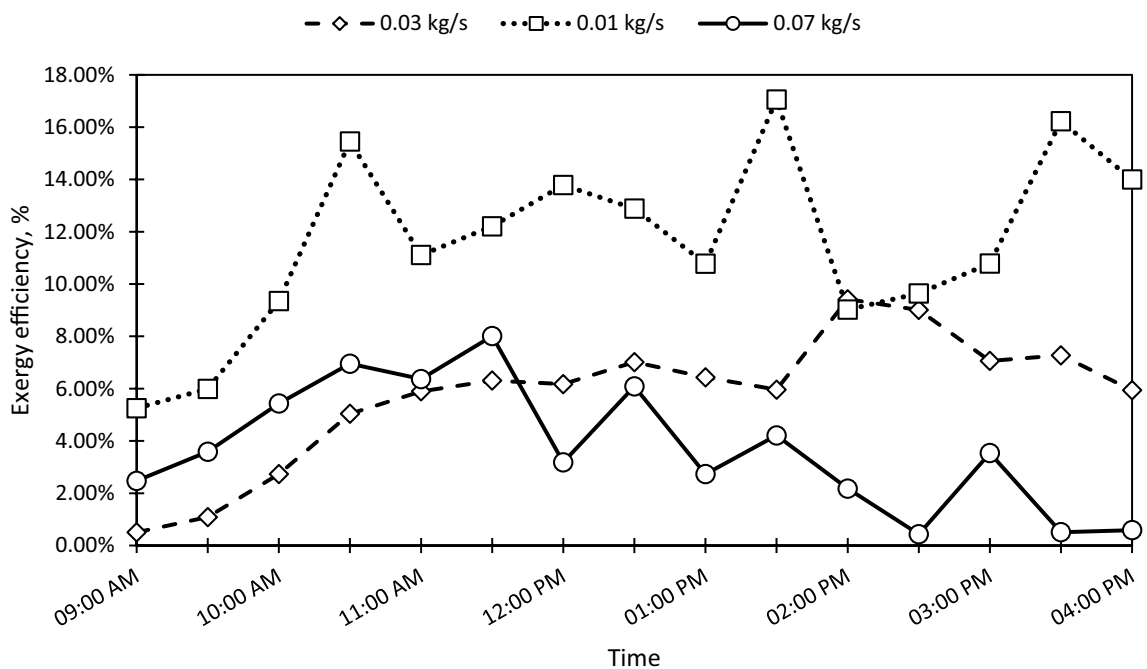


Fig. 9. Exergy efficiencies of FPSAC for three days.

enhanced convective heat transfer. The criteria for attaining optimal energy efficiency are consistent with the indoor testing outlined in Sect. 4.3.

Exergy performance of solar collector

Exergy analysis evaluates the quantity and quality of energy within the solar thermal system, providing a more accurate measure of real efficiency. The exergy efficiency of the FPSAC integrated with HSSF and baffles for air mass flow rates of 0.01 kg/s, 0.03 kg/s, and 0.07 kg/s is illustrated in Fig. 9 for Days 1 through 3. The overall trend indicates that fluctuations in exergy efficiencies during the day (from 9:00 AM to 4:00 PM) are influenced by solar irradiance levels, ambient temperature, and the collector’s temperature. The flow rate of 0.01 kg/s (Day 1) demonstrated the most significant variation and the highest overall exergy efficiency, with percentages fluctuating between 5.25% and 17.06%. The peak efficiency occurs at 1:30 PM with 17.06% on this particular day. On day 2 (0.03 kg/s), the exergy efficiency gradually increased, culminating in a notable spike

Mass flow rate, kg/s	Average exergy efficiency, %	Average exergy destruction, W
0.01	11.57	24.00
0.03	6.20	56.86
0.07	3.75	76.86

Table 6. Overview of exergy efficiency.

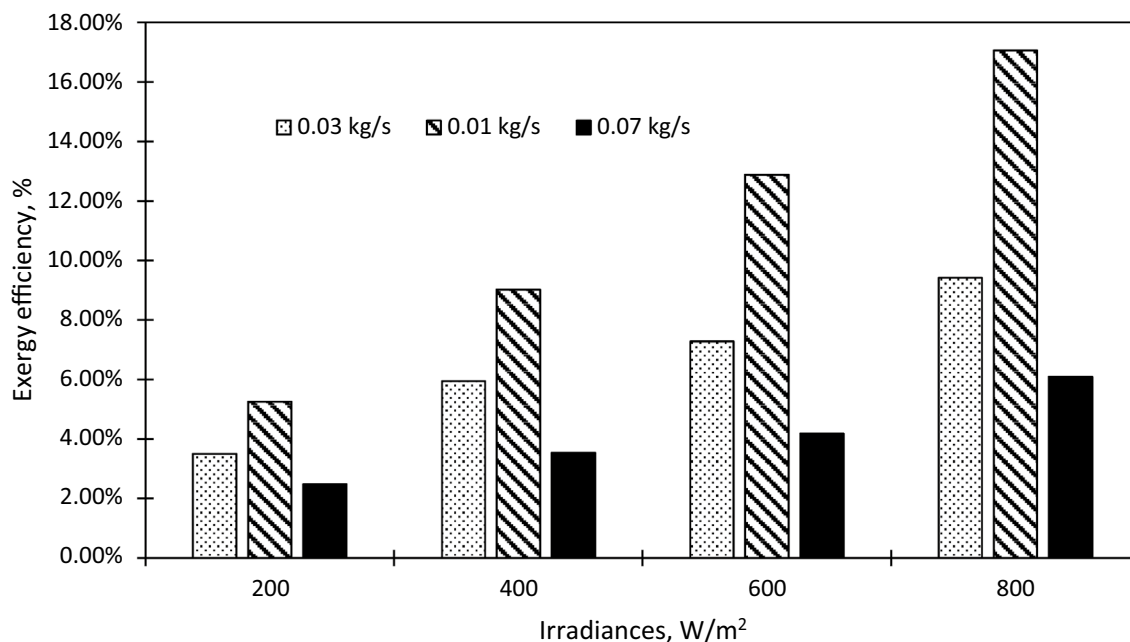


Fig. 10. Highest exergy efficiency across irradiance levels.

at 2:30 PM, reaching 16.11%, within a range of 0.55 to 16.11%. On Day 3 (0.07 kg/s), the experimental testing revealed the lowest exergy efficiency, which fluctuated between 0.51% and 6.95%, with a peak efficiency of 6.08% occurring at 10:30 AM. The ideal flow rate is discovered to be 0.01 kg/s, as it effectively balances adequate heat absorption with minimal thermal losses, thereby maximizing useful energy (exergy). Table 6 summarizes the exergy performance of each flow rate. The table demonstrates that the exergy efficiency decreases. The average exergy efficiency decreases as the mass flow rate increases, from 11.57% at 0.01 kg/s to 3.75% at 0.07 kg/s, as per the table. In contrast, the average exergy destruction experiences a substantial increase, rising from 24.00 W at 0.01 kg/s to 76.86 W at 0.07 kg/s. The reduction in exergy efficiency with increased flow rate is owing to the increased irreversibility within the solar collector system. The reasons for irreversibility come from heat loss and pressure drop inside the system. This underscores the increased irreversibility that occurs at higher flow rates.

Figure 10 is a bar chart illustrating the highest exergy efficiency values of FPSAC with HSSF and baffles at various flow rates (0.01 to 0.07 kg/s) and solar irradiance values spanning from 200 W/m² to 800 W/m². It is evident from the trend that increased solar irradiance results in increased exergy efficiency. Exergy efficiency increases with irradiance, with values of 3.5%, 5.25%, and 2.47% at 200 W/m² for 0.03 kg/s, 0.01 kg/s, and 0.07 kg/s, rising to 5.94%, 9.02%, and 3.54% at 400 W/m², 7.3%, 12.9%, and 4.18% at 600 W/m², and 9.42%, 17.06%, and 6.08% at 800 W/m² for the same mass flow rates. The optimal flow rate, which yields the highest overall exergy efficiency across all irradiance levels, is 0.01 kg/s. The experimental data indicate a maximal exergy efficiency of 17.06% within the irradiance range of 200–800 W/m² and a flow rate range of 0.01–0.07 kg/s. The air travels excessively through the collector, resulting in minimal temperature gain. Consequently, the potential for high-quality energy transfer is restricted. From a practical perspective, the flow rate should be optimized using the available solar irradiance. The most efficient performance is achieved using approximately 0.01 kg/s under moderate to high irradiance. These findings suggest that adaptive or variable flow management systems can significantly enhance solar air collector performance by maintaining near-optimal exergy efficiency throughout the day.

The effect of temperature difference variations on the thermal efficiencies

The relationship between temperature difference against thermal efficiency at varying solar irradiance levels and mass flow rates is illustrated in Fig. 11, an outdoor experimental graph. Thermal efficiency progressively increases as the temperature difference rises, with a range of approximately 13% at 3 °C to 30% at 20 °C under the minimal flow rate condition of 0.01 kg/s. Nevertheless, the efficacy is considerably enhanced at 0.03 kg/s,

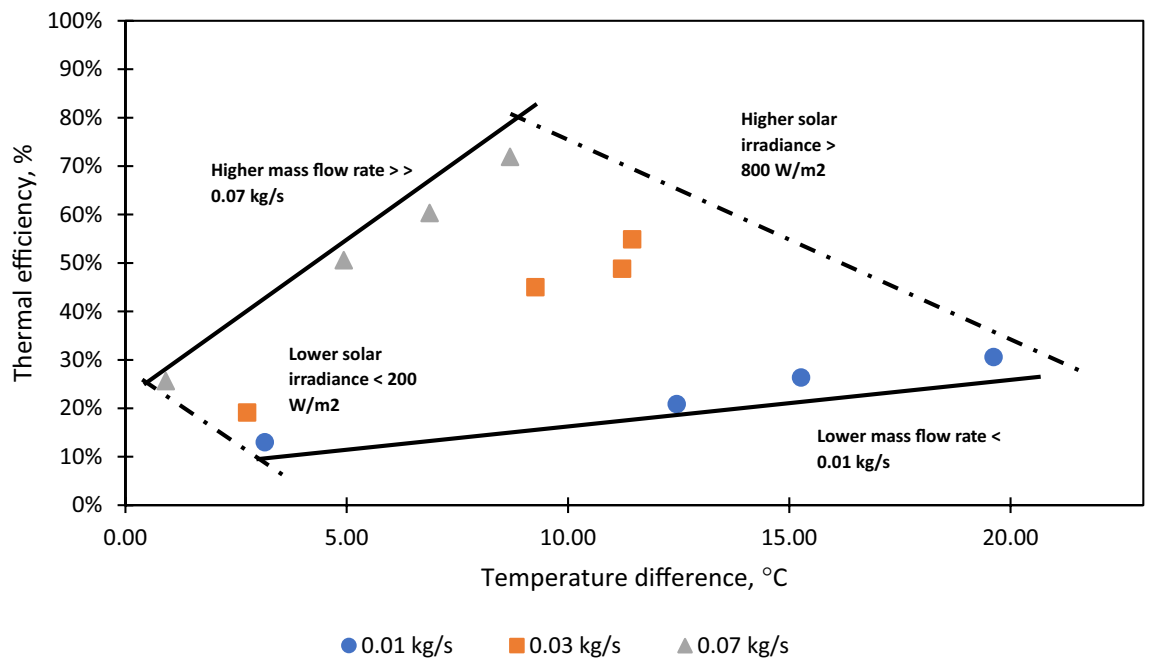


Fig. 11. Relationship between temperature difference and thermal efficiency.

with an approximate 55% increase at a 12 °C temperature variation. The highest thermal efficiencies are observed at an operating rate of 0.07 kg/s, with values ranging from 25 to 72% within a lower temperature fluctuation range of 1 °C to 9 °C. The synergistic effect of a high flow rate and a substantial solar input is demonstrated by these points, which correspond to higher solar irradiance levels exceeding 800 W/m². In contrast, the system's efficiency decreases to less than 25% at lower irradiance levels (<200 W/m²) despite moderate flow rates, underscoring the importance of adequate solar input for optimal performance. Generally, higher mass flow rates lead to improved heat extraction and a reduced temperature rise, whereas lower mass flow rates result in greater temperature differences but lower efficiencies.

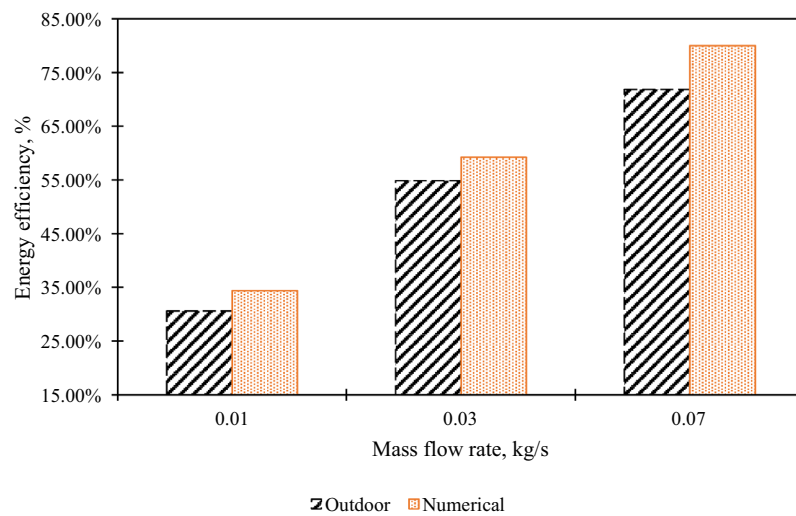
Validation analysis

The numerical results were used to validate the outdoor experiments of a solar air collector with hollow semi-stadium fins (HSSF) and baffles at irradiance levels of 400, 600, and 800 W/m², as shown in Fig. 12, with flow rates of 0.01, 0.03, and 0.07 kg/s. Both methods verified that fins and baffles enhanced energy efficiency by minimizing thermal losses and enhancing convective heat transfer. Outdoor experiments demonstrated efficiencies ranging from 30.58% to 71.91%, while numerical computations achieved efficiencies of 34.37% to 80.00% at 800 W/m². At 600 W/m², the outdoor values ranged from 26.36% to 60.33%, while the numerical values ranged from 32.71% to 69.39%. At 400 W/m², the outdoor efficiencies decreased to 20.88–50.57%, while the numerical values ranged from 23.58 to 53.20%. The performance was at its best at 800 W/m², moderate at 600 W/m², and at its lowest at 400 W/m², which demonstrates the significant impact of solar input. In conclusion, the findings substantiate the efficacy of baffles and fins as improvements to solar air collectors.

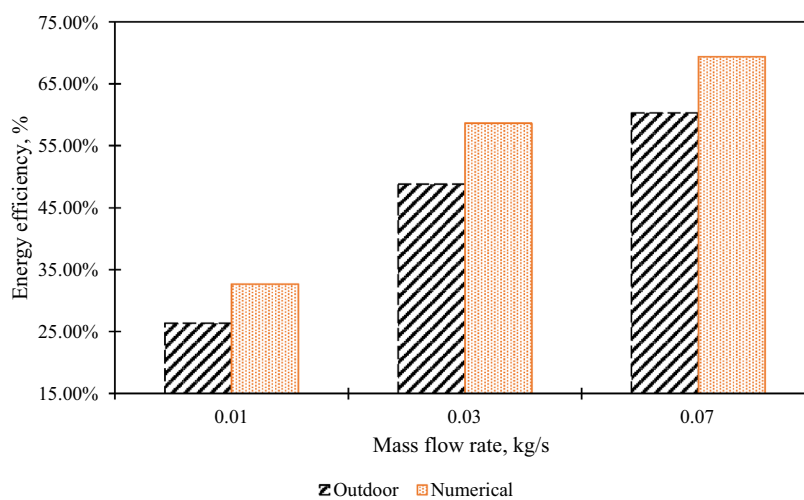
Comparison of the present study (outdoor) with prior studies

The comparison of thermal efficiency versus mass flow rate between the present outdoor study and prior works by P. Sudhakar and M. Cheralathan⁴⁶, as well as Kim et al.⁴⁷, is illustrated in the line graph in Fig. 13. In terms of average performance across all flow rates, the present study outperforms both referenced studies, demonstrating a consistent increase in efficiency from 30% at 0.01 kg/s to approximately 72% at 0.07 kg/s. In contrast, Sudhakar and Cheralathan⁴⁶ reported that efficiencies increased from 46% to approximately 63% within the same range. In contrast, Kim et al.⁴⁷ demonstrated significantly lower efficiencies, starting at 10% and achieving only approximately 44% at a flow rate of 0.07 kg/s. The superior performance of the present study can be attributed to the incorporation of cylindrical semi-stadium fins and baffles in the collector design, which likely enhanced heat transfer. This comparison confirms that the present study obtained an approximate 9% to 28% higher efficacy than the other two studies throughout the tested mass flow rate range. It can be proven that experimental validation, along with previous studies, validates the superior performance of the novel solar collector. The proposed solar collector design introduces the innovative HSSF with a multi-level array combined with baffles, which distinguishes its performance from previous research in solar thermal collectors.

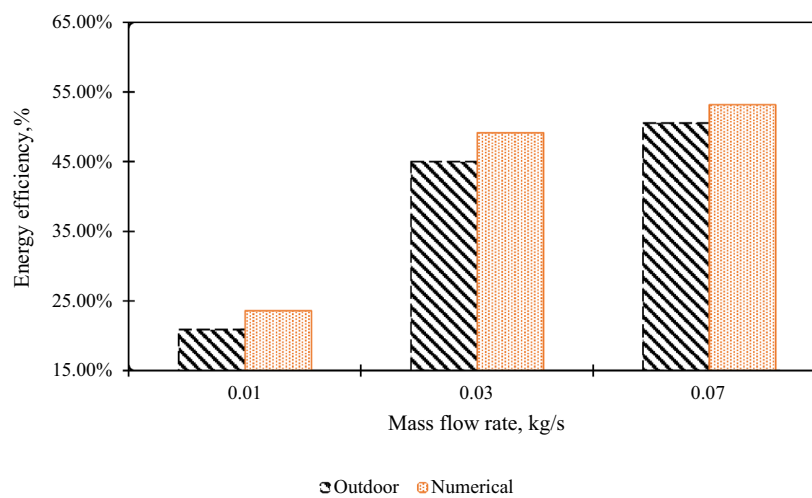
Beyond technical performance, the proposed solar air collector system affects economic feasibility, system integration, and long-term operational dependability. The improved energy and exergy efficiency reduced operating costs and consumption of energy. These impacts can provide a more cost-effective energy system of solar air collectors compared to the conventional system. Integrating this technology into existing infrastructure



a)



b)



c)

Fig. 12. Efficiency validation between outdoor and numerical results. (a) 800 W/m², (b) 600 W/m², and (c) 400 W/m².

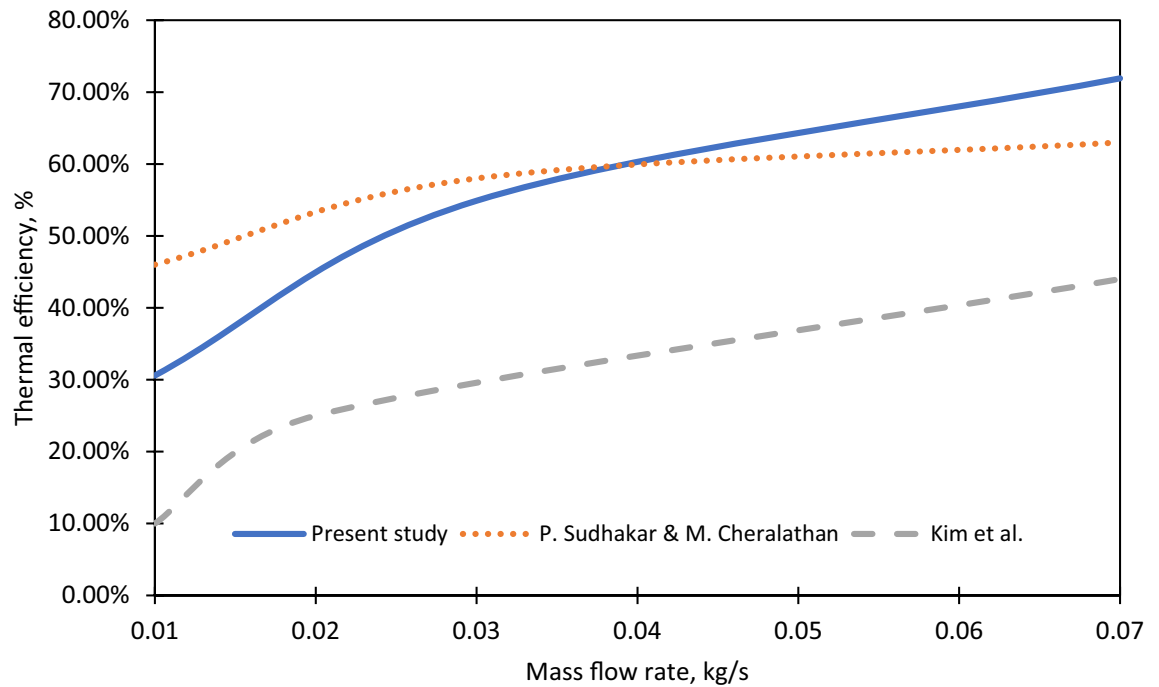


Fig. 13. Comparison of the outdoor experimental study with prior studies.

requires careful site-specific circumstances and retrofit procedures to address compatibility and scalability issues. Long-term dependability demands addressing material durability, maintenance, and performance stability over time to maintain efficiency and reduce lifetime costs. Incorporating these practical concerns into system design and assessment emphasizes its preparedness for real-world application and the need to address economic and operational variables to maximize sustainable energy deployment.

Conclusion

Both energy and exergy performances of the FPSAC were thoroughly examined using a multi-level array of hollow fins featuring a semi-stadium shape and baffles. The effectiveness of this configuration was validated through experimental and numerical testing, as well as a comparison with prior research. The research introduces a novel system design incorporating a multi-level HSSF and baffle setup, which substantially enhances the overall system performance. This novel configuration provides a sustainable and validated approach to advancing solar thermal energy applications. The collector system is tested in a real-time environment. The limitation of this study is that testing was conducted over a three-day period, which does not comprehensively reflect the long-term performance of the system under diverse weather and seasonal conditions. The research utilized air mass flow rates of 0.01 kg/s, 0.03 kg/s, and 0.07 kg/s, and was experimentally tested over three consecutive days. The performance is tested through two main components: energy and exergy components, with temperatures (outlet, bending, plate, and the differential between the inlet and outlet) of the solar collector. The performance is assessed based on different irradiance levels. This comprehensive analysis results in the following conclusions:

- The ambient temperatures and solar irradiation were recorded throughout the three days, ranging from 25 °C to 35.5 °C and from 86 W/m² to 939 W/m².
- The inlet-to-outlet differential temperatures for the respective flow rates were 21.80 °C at 0.01 kg/s, 12.24 °C at 0.03 kg/s, and 8.69 °C at 0.07 kg/s. The absorber plate and outlet temperatures, along with the temperature difference between the inlet and outlet, decrease as the mass flow rate increases from 0.01 to 0.07 kg/s, primarily due to enhanced convective heat transfer. The decrement in air residence duration within the collector is the primary cause of this effect.
- Testing at 0.07 kg/s on Day 3 yields the highest thermal efficiency (25.64%-71.91%), followed by 0.03 kg/s on Day 2 (19.145%-58.77%) and 0.01 kg/s on Day 1 (12.99%-30.58%). During outdoor testing, the maximum efficiency was 71.91% under an irradiance of 800 W/m² and an air flow rate of 0.07 kg/s, considering all irradiance levels and flow rate conditions.
- Generally, a reduction in mass flow rate gives a decreasing trend in exergy efficiency. At the condition flow value of 0.01 kg/s, the efficiency values ranged from 5.25% to 17.06%. At 0.03 kg/s, the efficiency varied between 0.55% and 9.42%, while at 0.07 kg/s, it spanned from 0.51% to 6.95%. The best possible efficiency was attained at the minimum flow rate (0.01 kg/s). Moreover, the maximum exergy efficiency recorded across all irradiance levels was 17.06%.
- The present research validates the effectiveness of the improved design by demonstrating superior efficiency in comparison to numerical and previous studies.

In brief, the HSSF's multi-level array configuration and the inclusion of baffles substantially enhance the efficient transformation of incoming energy into thermal output, establishing it as a practical solution for future solar energy projects. The practical deployment of the proposed solar air collector necessitates a range of approaches, including evaluation of economic viability, identification of integration challenges, and assurance of long-term reliability. It is recommended to integrate numerical data using artificial neural networks for thorough performance analysis and prediction. This will include doing both computational and experimental studies to assess the collector's energy, entropy, economic, and environmental parameters.

Data availability

The datasets used and/or analyzed during the current study are available from the corresponding Author on reasonable request.

Received: 10 October 2025; Accepted: 20 January 2026

Published online: 29 January 2026

References

- Ismail, F. B., Rahmat, M. A. A., Kazem, H. A., Al-Obaidi, A. S. M. & Ridwan, M. S. Maximizing energy via solar-powered smart irrigation: An approach utilizing a single-axis solar tracking mechanism. *Irrig. Drain.* <https://doi.org/10.1002/ird.2937> (2024).
- Ding, X. et al. A systematic review on liquid air energy storage system. *Renew. Sustain. Energy Rev.* **210**, 115164. <https://doi.org/10.1016/j.rser.2024.115164> (2025).
- Madadi Avargani, V., Zendejboudi, S., Osfouri, S. & Rostami, A. Performance evaluation of a solar nano-photocatalytic reactor for wastewater treatment applications: Reaction kinetics, CFD, and scale-up perspectives. *J. Clean. Prod.* **421**, 138240. <https://doi.org/10.1016/j.jclepro.2023.138240> (2023).
- Borode, A., Ahmed, N. & Olubambi, P. A review of solar collectors using carbon-based nanofluids. *J. Clean. Prod.* **241**, 118311. <https://doi.org/10.1016/j.jclepro.2019.118311> (2019).
- Ismail, F. B. et al. Malaysian rainwater harvesting system for in-house power generation. *Appl. Mech. Mater.* **922**, 123–134. <https://doi.org/10.4028/p-LjJFi0> (2024).
- Ahmad, A. et al. Parabolic trough solar collectors: A sustainable and efficient energy source. *Mater. Sci. Energy Technol.* **7**, 99–106. <https://doi.org/10.1016/j.mset.2023.08.002> (2024).
- Ding, X. et al. Energy, exergy, and economic analyses of a novel liquid air energy storage system with cooling, heating, power, hot water, and hydrogen cogeneration. *Energy Convers. Manag.* **305**, 118262. <https://doi.org/10.1016/j.enconman.2024.118262> (2024).
- Arroyo, A., Basurto, N., Casado-Vara, R., Timiraos, M. & Calvo-Rolle, J. L. A Hybrid Intelligent Modeling approach for predicting the solar thermal panel energy production. *Neurocomputing* **565**, 126997. <https://doi.org/10.1016/j.neucom.2023.126997> (2024).
- Din, S. I. U. et al. Thermohydraulic performance optimization of a novel double-pass solar air heater with vertical PCM-integrated cylinders: A comparative study. *Case Stud. Therm. Eng.* **71**, 106226. <https://doi.org/10.1016/j.csite.2025.106226> (2025).
- Afham Rahmat, M. A., Ibrahim, A., Aziat Ishak, M. A., Syafiq, U. & Al-Arife, K. M. Numerical investigation of thermal and airflow profiles in diverse solar dryer chamber configurations. *Case Stud. Therm. Eng.* **73**, 10661. <https://doi.org/10.1016/j.csite.2025.10661> (2025).
- Maarof, H. A. & Maree, I. E. Enhancing PV/T efficiency using PCM-integrated single-finned tube cooling system. *Int. J. Heat Fluid Flow* **117**, 110091. <https://doi.org/10.1016/j.ijheatfluidflow.2025.110091> (2026).
- Ahmad, T. & Zhang, D. A critical review of comparative global historical energy consumption and future demand: The story told so far. *Energy Rep.* **6**, 1973–1991. <https://doi.org/10.1016/j.egy.2020.07.020> (2020).
- Saygin, D., Kempener, R., Wagner, N., Ayuso, M. & Gielen, D. The Implications for renewable energy innovation of doubling the share of renewables in the global energy mix between 2010 and 2030. *Energies (Basel)* **8**(6), 5828–5865. <https://doi.org/10.3390/en8065828> (2015).
- Pongboriboon, N., Mariyappan, V., Wu, W. & Chandra-Ambhorn, W. Economic and environmental analyses for achieving net-zero CO₂ emissions of a green diesel production process. *J. Taiwan Inst. Chem. Eng.* **165**, 105781. <https://doi.org/10.1016/j.jtice.2024.105781> (2024).
- Olabi, A. G., et al. Progress in Solar Thermal Systems and Their Role in Achieving the Sustainable Development Goals. 2022, MDPI. <https://doi.org/10.3390/en15249501>.
- Ud Din, S. I. et al. Double-pass solar air heater with staggered vertical phase change material cylinders: Thermal performance evaluation. *Appl. Therm. Eng.* **274**, 126762. <https://doi.org/10.1016/j.applthermaleng.2025.126762> (2025).
- Maarof, H. A., Madadi Avargani, V., Maree, I. E. & Yaseen, A. H. CFD modeling of a tubular three-pass solar air heater with phase change material: Investigating heat transfer enhancement and energy efficiency. *J. Energy Storage* **87**, 11152. <https://doi.org/10.1016/j.est.2024.111522> (2024).
- Machi, M. H., Farkas, I. & Buzas, J. Enhancing thermal efficiency of double-pass solar air collectors: A comparative study on the role of V-angled perforated fins. *Energy Rep.* **12**, 481–494. <https://doi.org/10.1016/j.egy.2024.06.048> (2024).
- Rahmat, M. A. A. et al. Design and performance optimization of hollow semi-stadium fins (HSSF) at multi-level array configuration for solar air collector. *Int. Commun. Heat Mass Transf.* **166**, 109154. <https://doi.org/10.1016/j.icheatmasstransfer.2025.109154> (2025).
- Fudholi, A. & Sopian, K. A review of solar air flat plate collector for drying application. *Renew. Sustain. Energy Rev.* **102**, 333–345. <https://doi.org/10.1016/j.rser.2018.12.032> (2019).
- Azha, N. I. S., Hussin, H., Nasif, M. S. & Hussain, T. Thermal performance enhancement in flat plate solar collector solar water heater: A review. *MDPI AG* <https://doi.org/10.3390/PR8070756> (2020).
- Ho, C. D., Chang, H., Yeh, C. W., Ng, C. A. & Hsieh, P. C. Optimizing device performance of multi-pass flat-plate solar air heaters on various recycling configurations. *Energies* <https://doi.org/10.3390/en16062568> (2023).
- Belay, T. M. & Atnaw, S. M. CFD simulations and experimental investigation of a flat-plate solar air heater at different positions of inlet and outlet. *J. Renew. Energy* **2023**(1), 3911228. <https://doi.org/10.1155/2023/3911228> (2023).
- Bojarajan, A. K. et al. A holistic overview of sustainable energy technologies and thermal management in UAE: The path to net zero emissions. *Int. J. Thermofluids* **23**, 100758. <https://doi.org/10.1016/j.ijft.2024.100758> (2024).
- Afham Rahmat, M. A. et al. Revolutionizing drying chambers for sustainable energy technologies in food and agriculture: A comprehensive review. *Sustain. Energy Technol. Assess.* **75**, 104205. <https://doi.org/10.1016/j.seta.2025.104205> (2025).
- Obaideen, K. et al. On the contribution of solar energy to sustainable developments goals: Case study on Mohammed bin Rashid Al Maktoum Solar Park. *Int. J. Thermofluids* **12**, 100123. <https://doi.org/10.1016/j.ijft.2021.100123> (2021).
- Kumar, A. & Tiwari, A. K. Solar-assisted post-combustion carbon-capturing system retrofitted with coal-fired power plant towards net-zero future: A review. *J. CO₂ Util.* **65**, 102241 (2022). <https://doi.org/10.1016/j.jcou.2022.102241>.
- Yousef, B. A. A. et al. On the contribution of concentrated solar power (CSP) to the sustainable development goals (SDGs): A bibliometric analysis. *Energy Strategy Rev.* **52**, 101356. <https://doi.org/10.1016/j.esr.2024.101356> (2024).

29. Panda, S. N. et al. Solar energy's role in achieving sustainable development goals in agriculture. *Int. J. Environ. Climate Change* **14**(5), 10–31. <https://doi.org/10.9734/ijec/2024/v14i54167> (2024).
30. Akram, N. et al. Experimental investigations of the performance of a flat-plate solar collector using carbon and metal oxides based nanofluids. *Energy* **227**, 120452. <https://doi.org/10.1016/j.energy.2021.120452> (2021).
31. Din, S. I. U. et al. Thermal performance analysis of a double-pass solar air heater with lava rock as porous and sensible heat storage material. *J. Energy Storage* <https://doi.org/10.1016/j.est.2024.112564> (2024).
32. Rani, P. & Tripathy, P. P. Experimental investigation on heat transfer performance of solar collector with baffles and semicircular loops fins under varied air mass flow rates. *Int. J. Therm. Sci.* **178**, 107597. <https://doi.org/10.1016/j.ijthermalsci.2022.107597> (2022).
33. Jamal, I. et al. Enhancing performance in solar air channels: A numerical analysis of turbulent flow and heat transfer with novel shaped baffles. *Appl. Therm. Eng.* <https://doi.org/10.1016/j.applthermaleng.2024.123561> (2024).
34. Boussouar, G. et al. Study of the thermal performance of solar air collectors with and without perforated baffles. *Energies (Basel)* <https://doi.org/10.3390/en17153812> (2024).
35. Razali, S. N. et al. Superior thermal dissipation through natural convection in a passive cooling system using multidirectional tapered fin heat sinks (MTFHS). *Int. J. Renew. Energy Dev.* **14**(2), 370–380. <https://doi.org/10.61435/ijred.2025.60742> (2025).
36. Arun, M. Experimental investigation on energy and exergy analysis of solar water heating system using zinc oxide-based nanofluid. *Arab. J. Sci. Eng.* **48**(3), 3977–3988. <https://doi.org/10.1007/s13369-022-07369-1> (2023).
37. Brahma, B., Shukla, A. K. & Baruah, D. C. Energy, exergy, economic and environmental analysis of phase change material based solar dryer (PCMSD). *J. Energy Storage* **88**, 111490. <https://doi.org/10.1016/j.est.2024.111490> (2024).
38. Madadi, V., Rahimi, A. & Tavakoli, T. Particle Science and Technology Enhancement in energy and exergy efficiency of a solar receiver using suspended alumina nanoparticles (nanofluid) as heat transfer fluid. *J. Part. Sci. Technol.* <https://doi.org/10.22104/jpst.2015.81> (2015).
39. Chand, S., Chand, P. & Kumar Ghritlahre, H. Thermal performance enhancement of solar air heater using louvered fins collector. *Sol. Energy* **239**, 10–24. <https://doi.org/10.1016/j.solener.2022.04.046> (2022).
40. Ahmed, H. E. Optimization of thermal design of ribbed flat-plate fin heat sink. *Appl. Therm. Eng.* **102**, 1422–1432. <https://doi.org/10.1016/j.applthermaleng.2016.03.119> (2016).
41. Mann, G. W. & Eckels, S. Multi-objective heat transfer optimization of 2D helical micro-fins using NSGA-II. *Int. J. Heat Mass Transf.* **132**, 1250–1261. <https://doi.org/10.1016/j.ijheatmasstransfer.2018.12.078> (2019).
42. Ng, K. M., Adam, N. M., Inayatullah, O. & Kadir, M. Z. A. A. Assessment of solar radiation on diversely oriented surfaces and optimum tilts for solar absorbers in Malaysian tropical latitude. *Int. J. Energy Environ. Eng.* **5**(1), 5. <https://doi.org/10.1186/2251-6832-5-5> (2014).
43. Bin Ishak, M. A. A. et al. Exergy performance of a reversed circular flow jet impingement bifacial photovoltaic thermal (PVT) solar collector. *Case Stud. Therm. Eng.* **49**, 103322. <https://doi.org/10.1016/j.csite.2023.103322> (2023).
44. Madadi Avargani, V., Abdlla Maarof, H. & Zendejboudi, S. Multiphysics CFD modeling to assess performance of a perforated multi-plate indirect solar dryer with a V-corrugated absorber surface. *Appl. Therm. Eng.* **227**, 12038. <https://doi.org/10.1016/j.applthermaleng.2023.120387> (2023).
45. Maarof, H. A., Maree, I. E. & Jadallah, A. A. Multiphysics CFD modeling of an optimized double-pass PVT system with phase change materials and wavy fins for enhanced thermal and electrical efficiency. *J. Energy Storage* **118**, 116245. <https://doi.org/10.1016/j.est.2025.116245> (2025).
46. Sudhakar, P. & Cheralathan, M. Thermal performance enhancement of solar air collector using a novel V-groove absorber plate with pin-fins for drying agricultural products: An experimental study. *J. Therm. Anal. Calorim.* **140**(5), 2397–2408. <https://doi.org/10.1007/s10973-019-08952-9> (2020).
47. Kim, J. H. et al. Performance assessment of an air-type BIPVT collector with perforated baffles through indoor and outdoor experiments. *Energies* <https://doi.org/10.3390/en15103779> (2022).
48. Prasetyo, S. D. et al. Optimization of photovoltaic thermal collectors using fins: A Review of strategies for enhanced solar energy harvesting. *Math. Model. Eng. Probl.* **10**(4), 1235–1248. <https://doi.org/10.18280/mmep.100416> (2023).
49. Duffie, J. A. & Beckman, W. A. *Solar Engineering of Thermal Processes*. Wiley (2013).
50. Al-Aasam, A. B., Ibrahim, A., Sopian, K., Abdulsahib, B. & Dayer, M. Nanofluid-based photovoltaic thermal solar collector with nanoparticle-enhanced phase change material (nano-PCM) and twisted absorber tubes. *Case Stud. Therm. Eng.* **49**, 103299. <https://doi.org/10.1016/j.csite.2023.103299> (2023).
51. Imad Ud Din, S., Ibrahim, A., Fazlizan, A., Ishak, M. A. A. & Abd Hamid, A. S. Performance analysis of a novel photovoltaic thermal pvt double pass solar air heater with cylindrical PCM capsules using CFD. *Int. J. Renew. Energy Res.* <https://doi.org/10.20508/ijrer.v13i3.14136.g8814> (2023).
52. Madadi Avargani, V., Abdlla Maarof, H. & Zendejboudi, S. Enhancing thermal and exergetic performance of solar air heating systems with PCM-integrated finned obstacles. *Energy* **326**, 136149. <https://doi.org/10.1016/j.energy.2025.136149> (2025).
53. Jaber, M. et al. Energetic and exergetic investigation of an innovative solar collector: Experimental study. *Case Stud. Therm. Eng.* **74**, 106848. <https://doi.org/10.1016/j.csite.2025.106848> (2025).
54. Kalogirou, S. A., Karellas, S., Braimakis, K., Stanciu, C. & Badescu, V. Exergy analysis of solar thermal collectors and processes. *Prog. Energy Combust. Sci.* **56**, 106–137. <https://doi.org/10.1016/j.peccs.2016.05.002> (2016).
55. Kalogirou, S. A., Karellas, S., Badescu, V. & Braimakis, K. Exergy analysis on solar thermal systems: A better understanding of their sustainability. *Renew. Energy* **85**, 1328–1333. <https://doi.org/10.1016/j.renene.2015.05.037> (2016).
56. Ge, Z., Wang, H., Wang, H., Zhang, S. & Guan, X. Exergy analysis of flat plate solar collectors. *Entropy* **16**(5), 2549–2567. <https://doi.org/10.3390/e16052549> (2014).
57. Moshery, R., Chai, T. Y., Sopian, K., Fudholi, A. & Al-Waeli, A. H. A. Thermal performance of jet-impingement solar air heater with transverse ribs absorber plate. *Sol. Energy* **214**, 355–366. <https://doi.org/10.1016/j.solener.2020.11.059> (2021).
58. Pirasteh, G., Saidur, R., Rahman, S. M. A. & Rahim, N. A. A review on development of solar drying applications. *Renew. Sustain. Energy Rev.* **31**, 133–148. <https://doi.org/10.1016/j.rser.2013.11.052> (2014).

Acknowledgements

Sincerely, thank you to the Solar Thermal and Sustainable Technology Group, under the Sustainable Resources, Nature and Smart Living Cluster, University Research Group (KPU), and the Solar Energy Research Institute, Universiti Kebangsaan Malaysia, for their invaluable support and guidance throughout this project.

Author contributions

Muhammad Aqil Afham Rahmat : review & editing, Writing – original draft, Validation, Methodology, Investigation, Data curation, Conceptualization. Adnan Ibrahim: Writing – review & editing, Validation, Supervision, Project administration, Funding acquisition, Conceptualization. Khaled M. Al-Arife: Writing – review & editing, Validation, Supervision, Project administration, Funding acquisition, Conceptualization. Ubaidah Syafiq: Writing – review & editing, Validation, Supervision, Methodology, Data curation. Muhammad Amir

Aziat Ishak: Validation, Methodology, Data curation. Sahibzada Imad Ud Din: Validation, Methodology, Data curation. Mohamad Arif Mokhtar: Validation and Supervision. Norashikin Ahmad Ludin: Writing – review & editing, Validation, Supervision. Ahmad Fazlizan: Writing – review & editing, Validation, Supervision.

Funding

This research received no specific grant from any funding agency in the public, commercial, or not-for-profit sectors.

Declarations

Competing interests

The authors declare no competing interests.

Additional information

Correspondence and requests for materials should be addressed to A.I.

Reprints and permissions information is available at www.nature.com/reprints.

Publisher's note Springer Nature remains neutral with regard to jurisdictional claims in published maps and institutional affiliations.

Open Access This article is licensed under a Creative Commons Attribution-NonCommercial-NoDerivatives 4.0 International License, which permits any non-commercial use, sharing, distribution and reproduction in any medium or format, as long as you give appropriate credit to the original author(s) and the source, provide a link to the Creative Commons licence, and indicate if you modified the licensed material. You do not have permission under this licence to share adapted material derived from this article or parts of it. The images or other third party material in this article are included in the article's Creative Commons licence, unless indicated otherwise in a credit line to the material. If material is not included in the article's Creative Commons licence and your intended use is not permitted by statutory regulation or exceeds the permitted use, you will need to obtain permission directly from the copyright holder. To view a copy of this licence, visit <http://creativecommons.org/licenses/by-nc-nd/4.0/>.

© The Author(s) 2026